

Taming nuclear size and shape effects in superallowed β -decay

Bingcheng He¹,¹ Mikhail Gorchtein²,² Matthias Heinz^{3,4},^{3,4} Ben Ohayon⁵,⁵ Lucas Platter^{1,4},^{1,4} and Chien-Yeah Seng¹

¹*Department of Physics and Astronomy, University of Tennessee, Knoxville, TN 37996, USA*

²*PRISMA⁺⁺ Cluster of Excellence, Institut für Kernphysik, Johannes Gutenberg-Universität, Mainz, Germany*

³*National Center for Computational Sciences, Oak Ridge National Laboratory, Oak Ridge, TN 37831, USA*

⁴*Physics Division, Oak Ridge National Laboratory, Oak Ridge, TN 37831, USA*

⁵*Technion – Israel Institute of Technology, Haifa, Israel*

(Dated: May 15, 2026)

We present the first combined analysis of the statistical rate function f in superallowed β decays with *ab initio* calculations and data. We focus on $^{10}\text{C} \rightarrow ^{10}\text{B}^*$, $^{14}\text{O} \rightarrow ^{14}\text{N}^*$ and $^{26\text{m}}\text{Al} \rightarrow ^{26}\text{Mg}$, all of which are important channels for the precise determination of the Cabibbo-Kobayashi-Maskawa (CKM) matrix element V_{ud} . Nuclear charge form factors are obtained by combining experimental data on nuclear charge radii and theory calculations of ratios of moments with the in-medium similarity renormalization group, while the β decay form factors are derived from exact isospin relations. This enables a rigorous study of the nuclear shape dependence in the statistical rate function f and the quantification of its uncertainties from both experiment and theory. The calculation leads to a more precise test for the first-row CKM unitarity with reduced theoretical uncertainties. This work demonstrates a reliable strategy for combining nuclear many-body calculations with high-precision nuclear data to describe β decays at tree level for precision tests of the Standard Model.

Introduction – Superallowed $0^+ \rightarrow 0^+$ nuclear β decays are central to precision tests of the Standard Model (SM) [1–3], providing the most precise determination of the Cabibbo-Kobayashi-Maskawa (CKM) [4, 5] matrix element V_{ud} . CKM unitarity at the first row implies the vanishing of the quantity

$$\Delta_{\text{CKM}} \equiv |V_{ud}|^2 + |V_{us}|^2 + |V_{ub}|^2 - 1, \quad (1)$$

which is currently tested at the sub-permille level [6]. Any significant deviation of Δ_{CKM} from zero would signal physics beyond the SM. Great interest has been triggered, in particular, by the observation of a $\sim 3\sigma$ deviation of the first-row unitarity through a global fit of V_{ud} and V_{us} obtained from nuclear, neutron, pion, and kaon decays [7]. Moreover, the agreement of V_{ud} values from individual superallowed transitions constrains possible scalar interactions via the Fierz interference term [8–10].

A sub-permille extraction of V_{ud} from superallowed β decays requires precise knowledge of the $\mathcal{F}t$ value [6],

$$\mathcal{F}t = ft(1 + \delta'_R)(1 + \delta_{\text{NS}} - \delta_C), \quad (2)$$

where t is the partial half-life and f , δ'_R , δ_{NS} , and δ_C encode nuclear-structure-dependent effects. Here we focus on the statistical rate function [9, 11]

$$f = m_e^{-5} \int_{m_e}^{E_0} pE(E_0 - E)^2 F(E)C(E)Q(E)R(E)r(E) dE, \quad (3)$$

the phase-space integral of the β spectrum that includes the Fermi function F , shape factor C , atomic screening Q , kinematic recoil R , and atomic overlap r . The factors F and C depend on the nuclear size through the charge density $\rho_{\text{ch}}(r)$ and the transition density $\rho_{\text{cw}}(r)$, respectively. Earlier studies considered them as unrelated quantities using empirical parameterizations and the nuclear shell

model [9] or treated ρ_{cw} perturbatively [12, 13]. Recent studies uncovered isospin relations among them [14, 15]:

$$\begin{aligned} \rho_{\text{cw}} &= \rho_{\text{ch}}^1 + Z_0(\rho_{\text{ch}}^0 - \rho_{\text{ch}}^1) = \rho_{\text{ch}}^1 + (Z_{-1}/2)(\rho_{\text{ch}}^{-1} - \rho_{\text{ch}}^1) \\ 2Z_0\rho_{\text{ch}}^0 &= Z_1\rho_{\text{ch}}^1 + Z_{-1}\rho_{\text{ch}}^{-1}, \end{aligned} \quad (4)$$

where the superscript of ρ_{ch} and the subscript of the nuclear charge Z denotes the third isospin component T_z (with $T_z = 1/2$ for neutrons). This enables a data-driven treatment of nuclear size effects in f using measured charge radii. A reanalysis of the $^{26\text{m}}\text{Al} \rightarrow ^{26}\text{Mg}$ transition partially restored the first-row CKM unitarity [16].

High-precision charge radii from muonic atom and isotope shift measurements exist for only a small subset of superallowed emitters [17]. Moreover, beyond the radius, f depends on the detailed shape of the charge density $\rho_{\text{ch}}(r)$ encoded in the nuclear form factor at finite momentum transfer q^2 . This shape information usually comes from electron-nucleus scattering data, which are lacking for nearly all unstable nuclei (with recent progress at radioactive-ion-beam facilities [18]) and for many stable daughter nuclei [19]. It has been common to infer the density shape from the nearest stable isotope [9], introducing an additional uncontrolled approximation. As a result, the data-driven re-analysis of f could only be applied to 15 of the 23 measured superallowed transitions and carries substantial uncertainty from the assumed density shape [20].

Recent advances in *ab initio* nuclear theory offer a path forward. Chiral effective field theory (EFT) provides a systematic, order-by-order improvable framework for low-energy nuclear interactions [21, 22]. Many-body calculations based on chiral EFT Hamiltonians have progressed rapidly due to methodological developments and growing computational power [23], enabling *ab initio* studies from light to heavy nuclei, including both closed- and

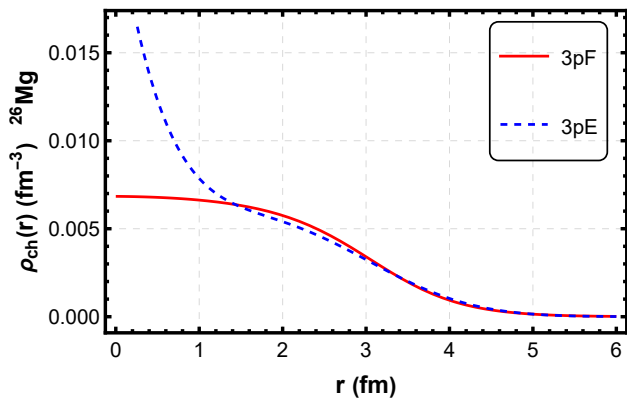


Figure 1. Nuclear charge density for ^{26}Mg in two different models with the first three moments fixed: $\langle r^2 \rangle = 9.1809 \text{ fm}^2$, $\langle r^4 \rangle = 125.521 \text{ fm}^4$, $\langle r^6 \rangle = 2204.11 \text{ fm}^6$.

open-shell systems [24–35]. In particular, the in-medium similarity renormalization group (IMSRG) [36, 37] has become a widely used *ab initio* method for nuclear-structure studies, including densities and form factors [38–41].

In this Letter, we establish a novel prescription for a high-precision, model-independent determination of f by combining experimental information on nuclear charge densities with *ab initio* calculations. The method applies to any superallowed decay for which at least one charge radius in the isotriplet is experimentally known. We illustrate its impact for $^{10}\text{C} \rightarrow ^{10}\text{B}^*$, $^{14}\text{O} \rightarrow ^{14}\text{N}^*$, and $^{26\text{m}}\text{Al} \rightarrow ^{26}\text{Mg}$: the first two are especially sensitive to new scalar interactions, while the third yields the most precise V_{ud} . For these cases, the *ab initio* determination of moment ratios reduces uncertainties in f from nuclear-size effects beyond the charge radii to below the 0.01% level. We provide a rigorous uncertainty analysis, discuss consequences for V_{ud} and CKM unitarity, and outline future opportunities, including connections to atomic-physics inputs and experimental efforts.

Model independence of f – Determining f requires the Fermi function $F(E)$, obtained by solving the Dirac equation for the outgoing positron in the static Coulomb potential generated by the charge density of the daughter nucleus, and the shape factor $C(E)$, computed from a charged weak density ρ_{cw} . Using isospin symmetry [Eq. (4)], ρ_{cw} can be fixed if an additional charge density in the isotriplet is known. Although the charge density can be obtained from a Fourier transform of the charge form factor $F_{\text{ch}}(q^2)$, it is highly sensitive to the extrapolation of F_{ch} to large q^2 [42], a region scarcely constrained by experiment and less reliably predicted by theory. Different large- q^2 extrapolations therefore imply different charge-density models, raising the key issue of the model dependence of f .

Recently, Ref. [43] showed that in highly-charged ions, fixing the three lowest moments $\langle r^{2,4,6} \rangle$ makes observables largely insensitive to the detailed charge-density

model: even very different densities can reproduce identical energy levels up to 10^{-5} accuracy. This allows for a model-independent extraction of nuclear charge radii from Li-like ions. We find that the same holds for the statistical rate function f . To illustrate this, we compare the standard three-parameter Fermi (3pF) charge density with an intentionally unrealistic three-parameter exponential (3pE) model (see Ref. [43] for definitions). Although Fig. 1 shows that the two densities differ strongly near the nuclear center while sharing the same $\langle r^{2,4,6} \rangle$, the resulting f values for the lightest (^{10}C) and heaviest ($^{26\text{m}}\text{Al}$) cases studied are nearly identical:

$$\begin{aligned} ^{10}\text{C} \rightarrow ^{10}\text{B}^* & : 2.30160 \text{ (3pF)} \text{ vs. } 2.30161 \text{ (3pE)}, \\ ^{26\text{m}}\text{Al} \rightarrow ^{26}\text{Mg} & : 478.027 \text{ (3pF)} \text{ vs. } 478.034 \text{ (3pE)}. \end{aligned}$$

The differences are $\leq 0.001\%$, well below our precision goal of 0.01% for V_{ud} , demonstrating that once $\langle r^{2,4,6} \rangle$ are fixed, f is essentially model independent. Consequently, the required nuclear-size input is reduced from the full density to its three lowest moments, which we determine precisely below by combining experimental information with *ab initio* calculations.

Ab initio calculations – We use the valence-space IMSRG (VS-IMSRG) [36, 37] to solve the many-body Schrödinger equation for nuclear Hamiltonians with two- and three-nucleon forces from chiral effective field theory. We consider two truncations of the VS-IMSRG equations: the VS-IMSRG(2), truncated at the normal-ordered two-body level, and the VS-IMSRG(3f₂), which approximately captures the leading effects of normal-ordered three-body operators [44]. We use three nuclear Hamiltonians: 1.8/2.0 (EM) [45], 1.8/2.0 (EM7.5) [38], and $\Delta\text{NNLO}_{\text{GO}}$ (with cutoff 394 MeV) [46]. This allows us to explore and quantify the uncertainty associated with the input nuclear interactions.

To compute charge-density moments, one can either construct the corresponding moment operators and evaluate them directly [33, 47], or, more conveniently, extract moments $\langle r^{2n} \rangle$ from derivatives of the charge form factor at low momentum transfer [40]. The operator approach becomes cumbersome for higher moments [48–50] and treats translational invariance only approximately due to particle-rank truncations [33]. Here we therefore compute $F_{\text{ch}}(q^2)$ with the VS-IMSRG at discrete low- q^2 points ($< 1 \text{ fm}^{-2}$) using

$$\begin{aligned} F_{\text{ch}}(q^2) = e \sum_{i=1}^A \left\{ G_E^i(q^2) \left(1 - \frac{q^2}{8m^2} \right) j_0(qr_i) \right. \\ \left. - \frac{q^2}{2m^2} \left[G_M^i(q^2) - \frac{1}{2} G_E^i(q^2) \right] (\ell_i \cdot \sigma_i) \frac{j_1(qr_i)}{qr_i} \right\}, \end{aligned} \quad (5)$$

where q is the momentum transfer, e the elementary charge, m the nucleon mass, $G_{E,M}^i$ the nucleon electric/magnetic form factors [51], ℓ_i and σ_i the orbital-

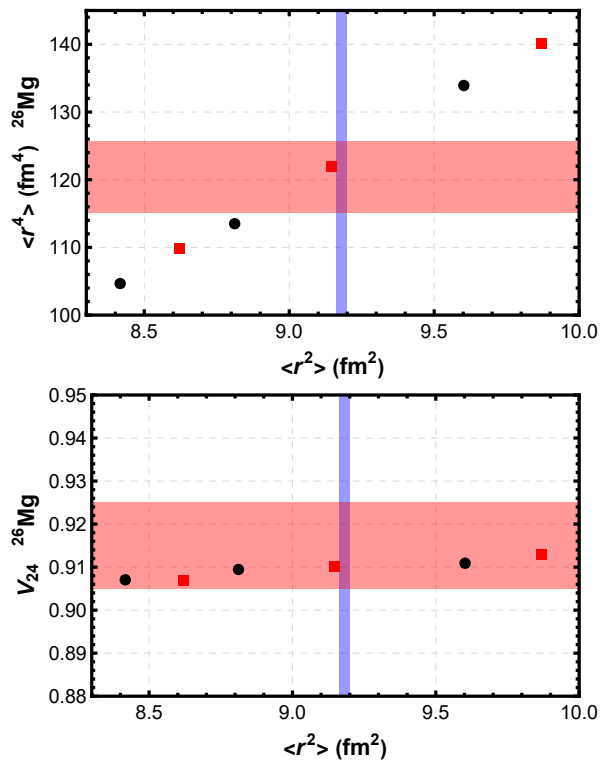


Figure 2. *Ab initio* predictions for $\langle r^2 \rangle$ vs. $\langle r^4 \rangle$ (upper panel) and $\langle r^2 \rangle$ vs. V_{24} (lower panel) for ^{26}Mg . Black dots indicate VS-IMSRG(2) results for three chiral EFT Hamiltonians, and red dots indicate VS-IMSRG(3f₂). Vertical and horizontal bands are experimental results obtained from muonic atom [54] and electron scattering [55], respectively. Uncertainty bands for the scattering results are derived from how the calculations converge as momentum transfer increases.

angular-momentum and spin operators, and $j_{0,1}$ spherical Bessel functions. The expression above accounts for nucleon-size, Darwin-Foldy, and spin-orbit corrections [40, 52]. To remove center-of-mass contamination and restore translational invariance, we correct the form factor using the Gaussian factorization of the center-of-mass wave function, established in coupled-cluster [53] and IMSRG calculations [39]:

$$F_{\text{ch}}^{\text{int}}(q^2) = e^{q^2 b_{\text{cm}}^2/4} F_{\text{ch}}(q^2), \quad (6)$$

where $F_{\text{ch}}^{\text{int}}(q^2)$ is the intrinsic charge form factor, $F_{\text{ch}}(q^2)$ is the calculated form factor that includes center-of-mass contamination, and b_{cm} is the oscillator length associated with center-of-mass motion, computed from the expectation value of the center-of-mass kinetic energy.

To assess theoretical accuracy, we compare the *ab initio* moment predictions with experiment. The top panel of Fig. 2 shows that VS-IMSRG results for absolute moments $\langle r^{2,4} \rangle$ depend strongly on the chosen Hamiltonian and truncation of the many-body method, implying sizable absolute uncertainties that are not competitive with experimental precision, particularly for $\langle r^2 \rangle$ from muonic

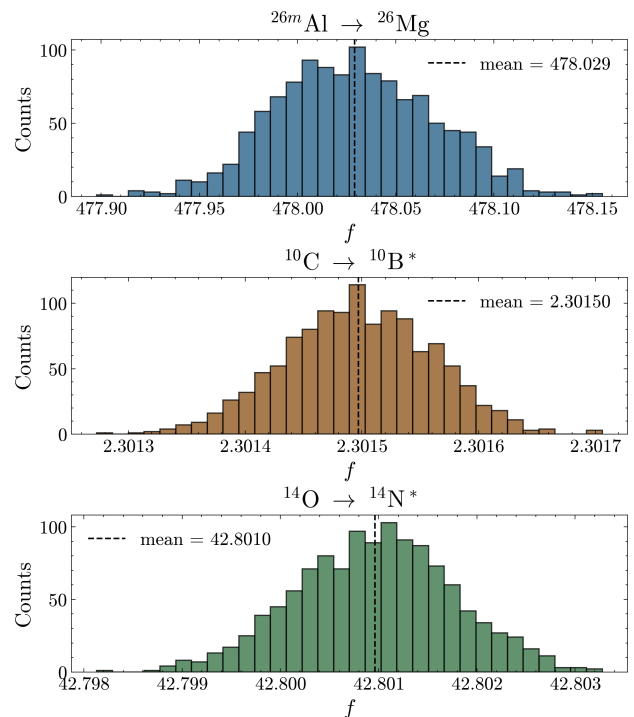


Figure 3. Histograms of sampled statistical rate functions f for the three transitions, obtained by propagating paired parent/daughter charge-density ensembles through the Coulomb-corrected phase-space calculation. Dashed lines indicate the sample means.

atoms. However, these uncertainties are correlated between moments [43], so the VS-IMSRG can predict the dimensionless moment ratios (“V-factors”) [56]

$$V_{2,2n} \equiv \langle r^2 \rangle^{1/2} / \langle r^{2n} \rangle^{1/2n}, \quad (7)$$

with high precision. This is evident in the lower panel of Fig. 2, where the calculated V_{24} in ^{26}Mg are fully consistent with electron-scattering results, but with a much smaller uncertainty. Therefore, the optimal strategy is to combine $\langle r^2 \rangle$ from muonic atoms and the V -factors from *ab initio* calculations. This allows us to obtain the moments $\langle r^{2,4,6} \rangle$ with maximum precision and minimize the density-shape related uncertainty of f .

This procedure also explains why we compute only the charge density ρ_{ch} (rather than the charged weak density ρ_{cw}) with *ab initio* methods. A reliable determination of ρ_{cw} requires external input for the mean square “charged weak radius” $\langle r^2 \rangle_{\text{cw}}$, which can only be extracted from high-precision measurements of nuclear-recoil effects in β decays (as in the BeEST experiment [57]); such measurements are not yet available for superallowed decays. Although one could infer $\langle r^2 \rangle_{\text{cw}}$ from charge radii using the isospin relation 4, it would not change our current strategy, which is to first deduce ρ_{ch} with *ab initio* methods and data and then obtain ρ_{cw} using isospin symmetry.

Data on nuclear charge radii – Our strategy requires

an experimental nuclear charge radius, typically available only for the stable $T_z = +1$ member of an isotriplet. However, the $T_z = -1$ charge radius can be inferred from the mirror-shift fit [54, 58], while the isospin formula yields the $T_z = 0$ charge radius. We adopt the compilation in Table 7 of Ref. [54]; the quoted uncertainties are comparable to those of the measured radii.

This procedure also enables a semi-empirical test of isospin symmetry by comparing the predicted $T_z = 0$ radius to available experimental data. Refs. [54, 59] find overall consistency with isospin symmetry, albeit with sizable uncertainties. A notable exception is $A = 26$, where the predicted ^{26}Al charge radius differs from the measured value by 5σ . This points towards a unique opportunity to probe large isospin breaking effects, achievable through an experimental measurement of the ^{26}Si charge radius. In this work, we adopt the experimental value of the ^{26}Al charge radius.

f -computation and uncertainty quantification – Using the procedure above, we compute the statistical rate function f for the superallowed decays of ^{10}C , ^{14}O , and ^{26}Al . For each transition, we construct the charge densities of the $T_z = 0, +1$ nuclei and obtain ρ_{cw} from isospin symmetry, then follow Ref. [16] to evaluate f .

We estimate uncertainties from charge-density inputs with two approaches. **Method 1:** We fix radii at their central values and vary the Hamiltonians and IMSRG truncations used to compute the V -factors; the spread in f quantifies the *ab initio* (i.e., V -factor) uncertainty. With V -factors fixed, we then vary the radii between the central and maximum values. This provides a straightforward assessment of the impact of each individual source of uncertainty. **Method 2:** We randomly sample a large ensemble of charge densities by varying both radii and V -factors within their uncertainties, compute f for each sample, and take the standard deviation of the resulting distribution (Fig. 3) as the combined uncertainty from the radii and *ab initio* calculations. For both methods, we include common uncertainties from Q_{EC} and atomic screening [60]. The outcomes from the two methods are in good agreement, and we quote the final results based on the more sophisticated Method 2 as follows:

$$\begin{aligned} ^{10}\text{C} \rightarrow ^{10}\text{B}^* &: f = 2.30150(71)_{Q_{\text{EC}}(43)_{\text{scr}}(6)_{\text{den}}} \\ ^{14}\text{O} \rightarrow ^{14}\text{N}^* &: f = 42.8010(77)_{Q_{\text{EC}}(63)_{\text{scr}}(8)_{\text{den}}} \\ ^{26}\text{Al} \rightarrow ^{26}\text{Mg} &: f = 478.029(101)_{Q_{\text{EC}}(82)_{\text{scr}}(40)_{\text{den}}}, \end{aligned}$$

where “den” is the charge density uncertainty, dominated by the charge radii. The V -factor contribution is $\mathcal{O}(0.001\%)$ or smaller, demonstrating that our procedure tightly constrains nuclear-size effects. Overall, we find a downward shift at the level of $\sim 0.01\%$ relative to the traditional evaluation [6], which did not incorporate the most precise charge density inputs or the correlation between ρ_{ch} and ρ_{cw} .

Implications for V_{ud} – We study the impact of our

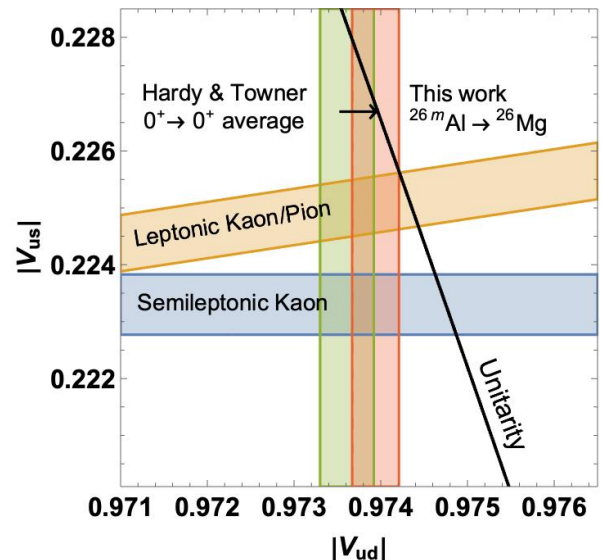


Figure 4. Updated plot of various V_{ud} and V_{us} determinations. The red vertical band represents our new result, $|V_{ud}| = 0.97394(27)$, using $\mathcal{F}t = 3070.16(1.68)$ from ^{26}Al decay. The green vertical band, $|V_{ud}| = 0.97373(31)$, is taken from Ref. [6]. The black line represents the unitarity condition $\Delta_{\text{CKM}} = 0$.

work on V_{ud} computed via [6]:

$$|V_{ud}|^2 = \frac{2984.431(3) s}{\mathcal{F}t(1 + \Delta_R^V)}, \quad (8)$$

using the transition $^{26}\text{Al} \rightarrow ^{26}\text{Mg}$, which alone returns a V_{ud} as precise as the global determination [16]. Δ_R^V is a nucleus-independent radiative correction that we take from Ref. [61]. We further account for recent studies of long-distance radiative corrections δ'_R at the $\mathcal{O}(Z\alpha^2)$ order in the EFT framework [62, 63], which increases the $\mathcal{F}t$ -value of this transition by 0.019%.

Figure 4 compares the value of V_{ud} obtained from ^{26}Al alone with that from the full set of superallowed decays, together with V_{us} and V_{us}/V_{ud} extracted from kaon and pion decays [7]. Our updated value of $|V_{ud}|$ from ^{26}Al implies $\Delta_{\text{CKM}} = \{-1.58(58), -0.79(60)\}$ (in units of 10^{-3}) when combined with V_{us} from semileptonic and leptonic kaon decays, respectively [7]. The corresponding unitarity tensions are 2.7 and 1.3σ . This should be compared with $\{-1.70(66), -0.93(69)\}$ from our previous work on ^{26}Al (corrected for the EFT shift) that did not include an *ab initio* calculation [16], for which the unitarity tensions were 2.6 and 1.3σ . We find that the central values of Δ_{CKM} decrease, while the substantially improved theoretical precision leaves the significance of the unitarity tension largely unchanged. This illustrates how a comprehensive treatment of nuclear-size effects can place the interpretation of new-physics searches in low-energy processes on a more solid footing.

Discussions and outlook – For SM tests using su-

perallowed β decays it is crucial to treat nuclear finite size accurately. Here, we have presented a systematic approach that combines charge radii data, mirror-shift parameterization, isospin symmetry, and *ab initio* charge form factors. We have shown that *ab initio* calculations predict dimensionless moment ratios (the V -factors) with high precision compared with absolute moments, and that f becomes essentially model independent once $\langle r^2 \rangle$, V_{24} , and V_{26} are fixed. For illustration, we have computed f for $^{10}\text{C} \rightarrow ^{10}\text{B}^*$, $^{14}\text{O} \rightarrow ^{14}\text{N}^*$, and $^{26\text{m}}\text{Al} \rightarrow ^{26}\text{Mg}$ with a rigorous uncertainty budget that substantially strengthens the test for the first-row CKM unitarity. Our prescription applies to 21 of the 23 measured superallowed transitions; the exceptions are $^{66}\text{As} \rightarrow ^{66}\text{Ge}$ and $^{70}\text{Br} \rightarrow ^{70}\text{Se}$, where no isotriplet charge radii are available. A full re-evaluation of f for the remaining transitions will be presented in follow-up work.

These results open several directions for future precision studies. First, the demonstrated stability of *ab initio* V -factor predictions suggests that they could provide key theory input for extracting charge radii from muonic atom energy levels [64], further improving determinations of f and fostering collaboration between nuclear *ab initio* and atomic physics communities. Second, because isospin symmetry is central to our framework, it should be tested experimentally, particularly in the $A = 26$ isotriplet that is pivotal for V_{ud} ; semi-empirical analyses predict sizable isospin breaking [54], which could be probed by measuring the ^{26}Si charge radius. Finally, our approach can complement the growing EFT program for electromagnetic effects in β decays [62, 63, 65–67] by helping constrain unknown low-energy constants in higher-order operators.

Acknowledgments – We thank Bob Wiringa, Garrett King and Saori Pastore for many useful discussions. BCH thanks Ragnar Stroberg for useful discussions and for facilitating access to computational resources at the Notre Dame Center for Research Computing. BCH acknowledges support from the National Science Foundation (NSF) FRHTP program under award No. PHY-2402275. The work of LP was supported by the National Science Foundation under Grant No. PHY-2412612) and the US Department of Energy (Contract No. DE-AC05-00OR22725). The work of CYS is supported in part by the U.S. Department of Energy Topical Collaboration “Nuclear Theory for New Physics,” award No. DE-SC0023663, and by the University of Tennessee, Knoxville. The work of MH was supported by the Laboratory Directed Research and Development Program of Oak Ridge National Laboratory, managed by UT-Battelle, LLC, for the U.S. Department of Energy and by the U.S. Department of Energy, Office of Science, Office of Advanced Scientific Computing Research and Office of Nuclear Physics, Scientific Discovery through Advanced Computing (SciDAC) program (SciDAC-5 NUCLEI). M.G. acknowledges support by the Deutsche Forschungsgemeinschaft (DFG) - GO 2604/3-2, Projektnummer 495329596, and by the Cluster

of Excellence “Precision Physics, Fundamental Interactions, and Structure of Matter” (PRISMA⁺⁺ EXC 2118/2) funded by the German Research Foundation (DFG) within the German Excellence Strategy (Project ID 390831469). This research used resources of the Oak Ridge Leadership Computing Facility located at Oak Ridge National Laboratory, which is supported by the Office of Science of the Department of Energy under contract No. DE-AC05-00OR22725.

-
- [1] S. L. Glashow, Partial-symmetries of weak interactions, *Nucl. Phys.* **22**, 579 (1961).
 - [2] A. Salam and J. C. Ward, Weak and electromagnetic interactions, *Nuovo Cim.* **11**, 568 (1959).
 - [3] S. Weinberg, A model of leptons, *Phys. Rev. Lett.* **19**, 1264 (1967).
 - [4] N. Cabibbo, Unitary Symmetry and Leptonic Decays, *Phys. Rev. Lett.* **10**, 531 (1963).
 - [5] M. Kobayashi and T. Maskawa, CP Violation in the Renormalizable Theory of Weak Interaction, *Prog. Theor. Phys.* **49**, 652 (1973).
 - [6] J. C. Hardy and I. S. Towner, Superallowed $0^+ \rightarrow 0^+$ nuclear β decays: 2020 critical survey, with implications for V_{ud} and CKM unitarity, *Phys. Rev. C* **102**, 045501 (2020).
 - [7] V. Cirigliano, A. Crivellin, M. Hoferichter, and M. Moulson, Scrutinizing CKM unitarity with a new measurement of the $K_{\mu 3}/K_{\mu 2}$ branching fraction, *Phys. Lett. B* **838**, 137748 (2023), [arXiv:2208.11707](https://arxiv.org/abs/2208.11707).
 - [8] J. D. Jackson, S. B. Treiman, and H. W. Wyld, Possible tests of time reversal invariance in Beta decay, *Phys. Rev.* **106**, 517 (1957).
 - [9] J. C. Hardy and I. S. Towner, Superallowed $0^+ \rightarrow 0^+$ nuclear beta decays: A Critical survey with tests of CVC and the standard model, *Phys. Rev. C* **71**, 055501 (2005), [arXiv:nucl-th/0412056](https://arxiv.org/abs/nucl-th/0412056).
 - [10] J. C. Hardy and I. S. Towner, New limit on fundamental weak-interaction parameters from superallowed beta decay, *Phys. Rev. Lett.* **94**, 092502 (2005), [arXiv:nucl-th/0412050](https://arxiv.org/abs/nucl-th/0412050).
 - [11] J. C. Hardy and I. S. Towner, Superallowed $0^+ \rightarrow 0^+$ nuclear beta decays: A New survey with precision tests of the conserved vector current hypothesis and the standard model, *Phys. Rev. C* **79**, 055502 (2009), [arXiv:0812.1202](https://arxiv.org/abs/0812.1202).
 - [12] D. H. Wilkinson, Methodology for superallowed Fermi beta decay. 2. Reduction of data, *Nucl. Instrum. Meth. A* **335**, 182 (1993).
 - [13] L. Hayen, N. Severijns, K. Bodek, D. Rozpedzik, and X. Mougeot, High precision analytical description of the allowed β spectrum shape, *Rev. Mod. Phys.* **90**, 015008 (2018), [arXiv:1709.07530](https://arxiv.org/abs/1709.07530).
 - [14] C.-Y. Seng and M. Gorchtein, Electroweak nuclear radii constrain the isospin breaking correction to V_{ud} , *Phys. Lett. B* **838**, 137654 (2023), [arXiv:2208.03037](https://arxiv.org/abs/2208.03037).
 - [15] C.-Y. Seng, Model-Independent Determination of Nuclear Weak Form Factors and Implications for Standard Model Precision Tests, *Phys. Rev. Lett.* **130**, 152501 (2023), [arXiv:2212.02681](https://arxiv.org/abs/2212.02681).
 - [16] M. Gorchtein, V. Katyal, B. Ohayon, B. K. Sahoo, and C.-

- Y. Seng, Cabibbo-Kobayashi-Maskawa unitarity deficit reduction via finite nuclear size, *Phys. Rev. Res.* **7**, L042002 (2025), [arXiv:2502.17070](#).
- [17] I. Angeli and K. P. Marinova, Table of experimental nuclear ground state charge radii: An update, *Atom. Data Nucl. Data Tabl.* **99**, 69 (2013).
- [18] K. Tsukada, Y. Abe, A. Enokizono, T. Goke, M. Hara, Y. Honda, T. Hori, S. Ichikawa, Y. Ito, K. Kurita, C. Legris, Y. Maehara, T. Ohnishi, R. Ogawara, T. Suda, T. Tamae, M. Wakasugi, M. Watanabe, and H. Wauke, First observation of electron scattering from online-produced radioactive target, *Phys. Rev. Lett.* **131**, 092502 (2023).
- [19] H. de Vries, C. W. de Jager, and C. de Vries, Nuclear charge and magnetization density distribution parameters from elastic electron scattering, *Atom. Data Nucl. Data Tabl.* **36**, 495 (1987).
- [20] C.-Y. Seng and M. Gorchtein, Data-driven re-evaluation of ft -values in superallowed beta decays, [arXiv:2309.16893](#).
- [21] E. Epelbaum, H.-W. Hammer, and U.-G. Meißner, Modern theory of nuclear forces, *Rev. Mod. Phys.* **81**, 1773 (2009).
- [22] R. Machleidt and D. Entem, Chiral effective field theory and nuclear forces, *Phys. Rep.* **503**, 1 (2011).
- [23] H. Hergert, A guided tour of ab initio nuclear many-body theory, *Front. Phys.* **8** (2020).
- [24] G. B. King, L. Andreoli, S. Pastore, M. Piarulli, R. Schiavilla, R. B. Wiringa, J. Carlson, and S. Gandolfi, Chiral Effective Field Theory Calculations of Weak Transitions in Light Nuclei, *Phys. Rev. C* **102**, 025501 (2020), [arXiv:2004.05263](#).
- [25] S. R. Stroberg, J. D. Holt, A. Schwenk, and J. Simonis, Ab initio limits of atomic nuclei, *Phys. Rev. Lett.* **126**, 022501 (2021), [arXiv:1905.10475](#).
- [26] B. Hu, W. Jiang, T. Miyagi, Z. Sun, A. Ekström, C. Forssén, G. Hagen, J. D. Holt, T. Papenbrock, S. R. Stroberg, and I. Vernon, Ab initio predictions link the neutron skin of ^{208}Pb to nuclear forces, *Nature Physics* **18**, 1196 (2022).
- [27] M. Frosini, T. Duguet, J.-P. Ebran, B. Bally, T. Mongelli, T. R. Rodríguez, R. Roth, and V. Somà, Multi-reference many-body perturbation theory for nuclei: II. Ab initio study of neon isotopes via PGCM and IM-NCSM calculations, *Eur. Phys. J. A* **58**, 63 (2022), [arXiv:2111.00797](#).
- [28] K. Hebeler, V. Durant, J. Hoppe, M. Heinz, A. Schwenk, J. Simonis, and A. Tichai, Normal ordering of three-nucleon interactions for ab initio calculations of heavy nuclei, *Phys. Rev. C* **107**, 024310 (2023).
- [29] A. Belley, J. M. Yao, B. Bally, J. Pitcher, J. Engel, H. Hergert, J. D. Holt, T. Miyagi, T. R. Rodríguez, A. M. Romero, S. R. Stroberg, and X. Zhang, Ab initio uncertainty quantification of neutrinoless double-beta decay in ^{76}Ge , *Phys. Rev. Lett.* **132**, 182502 (2024).
- [30] S. Elhatisari, L. Bovermann, Y.-Z. Ma, E. Epelbaum, D. Frame, *et al.*, Wavefunction matching for solving quantum many-body problems, *Nature* **630**, 59 (2024), [arXiv:2210.17488](#).
- [31] A. Tichai, P. Demol, and T. Duguet, Towards heavy-mass ab initio nuclear structure: Open-shell Ca, Ni and Sn isotopes from Bogoliubov coupled-cluster theory, *Phys. Rev. Lett.* **B 851**, 138571 (2024), [arXiv:2307.15619](#).
- [32] Z. H. Sun, A. Ekström, C. Forssén, G. Hagen, G. R. Jansen, and T. Papenbrock, Multiscale physics of atomic nuclei from first principles, *Phys. Rev. X* **15**, 011028 (2025), [arXiv:2404.00058](#).
- [33] M. Door, C.-H. Yeh, M. Heinz, F. Kirk, C. Lyu, *et al.*, Probing new bosons and nuclear structure with ytterbium isotope shifts, *Phys. Rev. Lett.* **134**, 063002 (2025), [arXiv:2403.07792](#).
- [34] F. Bonaiti, G. Hagen, and T. Papenbrock, Structure of the doubly magic nuclei ^{208}Pb and ^{266}Pb from ab initio computations, [arXiv:2508.14217](#).
- [35] K. B. Ng, S. Foster, L. Cheng, P. Navratil, and S. Malbrunot-Ettenauer, Nuclear Schiff Moment of the Fluorine Isotope ^{19}F , *Phys. Rev. Lett.* **136**, 112501 (2026), [arXiv:2507.19811](#).
- [36] H. Hergert, S. Bogner, T. Morris, A. Schwenk, and K. Tsukiyama, The in-medium similarity renormalization group: A novel ab initio method for nuclei, *Phys. Rep.* **621**, 165 (2016).
- [37] S. R. Stroberg, H. Hergert, S. K. Bogner, and J. D. Holt, Nonempirical interactions for the nuclear shell model: An update, *Ann. Rev. Nucl. Part. Sci.* **69**, 307 (2019).
- [38] P. Arthuis, K. Hebeler, and A. Schwenk, Neutron-rich nuclei and neutron skins from chiral low-resolution interactions, [arXiv:2401.06675](#).
- [39] M. Heinz, M. Hoferichter, T. Miyagi, F. Noël, and A. Schwenk, Ab initio calculations of overlap integrals for $\mu \rightarrow e$ conversion in nuclei, *Phys. Lett. B* **871**, 139975 (2025).
- [40] T. Miyagi, M. Heinz, and A. Schwenk, Ab initio computations of the fourth-order charge density moments of ^{48}Ca and ^{208}Pb , *Phys. Lett. B* **872**, 140032 (2026).
- [41] Y. Hijikata, J. Zenihiro, S. Terashima, Y. Matsuda, H. Sakaguchi, P. Arthuis, T. Miyagi, S. Ota, *et al.*, First Extraction of the Matter Radius of ^{132}Sn via Proton Elastic Scattering at 200 MeV/Nucleon, *Prog. Theor. Exp. Phys.* **2026**, 013D02 (2026), [arXiv:2602.08455](#).
- [42] F. Noël and M. Hoferichter, Uncertainty quantification for $\mu \rightarrow e$ conversion in nuclei: charge distributions, *J. High Energy Phys.* **08**, 052, [arXiv:2406.06677](#).
- [43] V. A. Yerokhin and B. Ohayon, Model-independent determination of nuclear charge radii from Li-like ions, *Phys. Rev. A* **113**, 012804 (2026), [arXiv:2510.27427](#).
- [44] B. C. He and S. R. Stroberg, Factorized approximation to the in-medium similarity renormalization group IM-SRG(3), *Phys. Rev. C* **110**, 044317 (2024).
- [45] K. Hebeler, S. K. Bogner, R. J. Furnstahl, A. Nogga, and A. Schwenk, Improved nuclear matter calculations from chiral low-momentum interactions, *Phys. Rev. C* **83**, 031301(R) (2011).
- [46] W. G. Jiang, A. Ekström, C. Forssén, G. Hagen, G. R. Jansen, and T. Papenbrock, Accurate bulk properties of nuclei from $A = 2$ to ∞ from potentials with Δ isobars, *Phys. Rev. C* **102**, 054301 (2020).
- [47] G. Hagen, A. Ekström, C. Forssén, G. R. Jansen, W. Nazarewicz, T. Papenbrock, K. A. Wendt, S. Bacca, N. Barnea, B. Carlsson, C. Drischler, K. Hebeler, M. Hjorth-Jensen, M. Miorelli, G. Orlandini, A. Schwenk, and J. Simonis, Neutron and weak-charge distributions of the ^{48}Ca nucleus, *Nature Physics* **12**, 186 (2016).
- [48] T. Miyagi, Nuclear radii from first principles, *Front. Phys.* **13**, 1581854 (2025).
- [49] H. Kurasawa and T. Suzuki, The n th-order moment of the nuclear charge density and contribution from the neutrons, *Prog. Theor. Exp. Phys.* **2019**, 113D01 (2019).
- [50] T. Naito, G. Colò, H. Liang, and X. Roca-Maza, Second and fourth moments of the charge density and neutron-

- skin thickness of atomic nuclei, *Phys. Rev. C* **104**, 024316 (2021).
- [51] Z. Ye, J. Arrington, R. J. Hill, and G. Lee, Proton and neutron electromagnetic form factors and uncertainties, *Phys. Lett. B* **777**, 8 (2018).
- [52] H. Krebs, Nuclear currents in chiral effective field theory, *Eur. Phys. J. A* **56**, 234 (2020).
- [53] G. Hagen, T. Papenbrock, and D. J. Dean, Solution of the center-of-mass problem in nuclear structure calculations, *Phys. Rev. Lett.* **103**, 062503 (2009).
- [54] B. Ohayon, Critical evaluation of reference charge radii and applications in mirror nuclei, *Atom. Data Nucl. Data Tabl.* **165**, 101732 (2025), [arXiv:2409.08193](https://arxiv.org/abs/2409.08193).
- [55] R. Soundranayagam, A. Saha, K. K. Seth, C. W. de Jager, H. de Vries, H. Blok, and G. van der Steenhoven, Ground state charge distribution of ^{26}Mg , *Phys. Lett. B* **212**, 13 (1988).
- [56] G. Fricke, C. Bernhardt, K. Heilig, L. A. Schaller, L. Schellenberg, E. B. Shera, and C. W. de Jager, Nuclear Ground State Charge Radii from Electromagnetic Interactions, *Atom. Data Nucl. Data Tabl.* **60**, 177 (1995).
- [57] K. G. Leach and S. Friedrich (BeEST), The BeEST Experiment: Searching for Beyond Standard Model Neutrinos Using ^7Be Decay in STJs, *J. Low Temp. Phys.* **209**, 796 (2022), [arXiv:2112.02029](https://arxiv.org/abs/2112.02029).
- [58] S. J. Novario, D. Lonardonì, S. Gandolfi, and G. Hagen, Trends of Neutron Skins and Radii of Mirror Nuclei from First Principles, *Phys. Rev. Lett.* **130**, 032501 (2023), [arXiv:2111.12775](https://arxiv.org/abs/2111.12775).
- [59] V. Katyal, A. Chakraborty, B. K. Sahoo, B. Ohayon, C.-Y. Seng, M. Gorchtein, and J. Behr, Testing for isospin symmetry breaking by combining isotope shift measurements with precise calculations in potassium, *Phys. Rev. A* **111**, 042813 (2025), [arXiv:2412.05932](https://arxiv.org/abs/2412.05932).
- [60] The uncertainty of the atomic screening correction was taken to be 10% of its actual size, following the treatment in Ref. [20]. This is an extremely conservative estimate and should by no means hinder future efforts to reduce uncertainties from other sources, such as improved measurements of Q_{EC} values.
- [61] M. Gorchtein and C.-Y. Seng, The Standard Model Theory of Neutron Beta Decay, *Universe* **9**, 422 (2023), [arXiv:2307.01145](https://arxiv.org/abs/2307.01145).
- [62] Ò. L. Crosas and E. Mereghetti, Radiative corrections to superallowed beta decays at $\mathcal{O}(\alpha^2 Z)$, *J. High Energy Phys.* **02**, 114, [arXiv:2511.05481](https://arxiv.org/abs/2511.05481).
- [63] Z. Cao, R. J. Hill, R. Plestid, and P. Vander Griend, The $Z\alpha^2$ correction to superallowed beta decays in effective field theory and implications for $|V_{ud}|$, [arXiv:2511.05446](https://arxiv.org/abs/2511.05446).
- [64] I. Angeli *et al.*, Towards better nuclear charge radii, [arXiv:2604.08985](https://arxiv.org/abs/2604.08985).
- [65] R. J. Hill and R. Plestid, Field Theory of the Fermi Function, *Phys. Rev. Lett.* **133**, 021803 (2024), [arXiv:2309.07343](https://arxiv.org/abs/2309.07343).
- [66] R. J. Hill and R. Plestid, All orders factorization and the Coulomb problem, *Phys. Rev. D* **109**, 056006 (2024), [arXiv:2309.15929](https://arxiv.org/abs/2309.15929).
- [67] K. Borah, R. J. Hill, and R. Plestid, Renormalization of beta decay at three loops and beyond, *Phys. Rev. D* **109**, 113007 (2024), [arXiv:2402.13307](https://arxiv.org/abs/2402.13307).
- [68] S. R. White, Numerical canonical transformation approach to quantum many-body problems, *J. Chem. Phys.* **117**, 7472 (2002).
- [69] M. Heinz, A. Tichai, J. Hoppe, K. Hebeler, and A. Schwenk, In-medium similarity renormalization group with three-body operators, *Phys. Rev. C* **103**, 044318 (2021).
- [70] S. R. Stroberg, T. D. Morris, and B. C. He, In-medium similarity renormalization group with flowing 3-body operators, and approximations thereof, *Phys. Rev. C* **110**, 044316 (2024).
- [71] M. Heinz, T. Miyagi, S. R. Stroberg, A. Tichai, K. Hebeler, and A. Schwenk, Improved structure of calcium isotopes from ab initio calculations, *Phys. Rev. C* **111**, 034311 (2025).
- [72] T. D. Morris, N. M. Parzuchowski, and S. K. Bogner, Magnus expansion and in-medium similarity renormalization group, *Phys. Rev. C* **92**, 034331 (2015), [arXiv:1507.06725](https://arxiv.org/abs/1507.06725).
- [73] M. Heinz, Computational schemes for the Magnus expansion of the in-medium similarity renormalization group, *Phys. Rev. C* **113**, L041301 (2026).
- [74] T. Miyagi, NuHAMIL: A numerical code to generate nuclear two- and three-body matrix elements from chiral effective field theory, *Eur. Phys. J. A* **59**, 150 (2023), [arXiv:2302.07962](https://arxiv.org/abs/2302.07962).
- [75] J. Hoppe, A. Tichai, M. Heinz, K. Hebeler, and A. Schwenk, Natural orbitals for many-body expansion methods, *Phys. Rev. C* **103**, 014321 (2021).

SUPPLEMENTARY INFORMATION

Details of IMSRG calculations

In this section, we provide the technical details of the IMSRG method, including its setup and the calculation of nuclear charge form factors.

Method

We use VS-IMSRG [36, 37] to solve the many-body Schrödinger equation. This method solves for a unitary transformation of a given Hamiltonian H to decouple subspaces of the full A -body Hilbert space. Specifically, it decouples a core and valence space from the rest of the Hilbert space, yielding effective interactions and operators that can be solved using shell model techniques.

The similarity renormalization group transforms the Hamiltonian like

$$H(s) \equiv U(s)HU^\dagger(s), \quad (\text{S1})$$

where $U(s)$ is the unitary transformation as a function of the flow parameter s , with $U(0) = 1$. The aim is to obtain a unitary transformation such that as s increases the off-diagonal piece is suppressed, $H^{\text{od}}(s) \rightarrow 0$, where “off-diagonal” refers to the part of the Hamiltonian to be decoupled. To achieve this, we specify an anti-Hermitian generator η that evolves the transformation in s ,

$$\frac{d}{ds}U(s) = \eta(s)U(s). \quad (\text{S2})$$

There is some freedom in choosing the form of η , and several choices have been used in the literature. Here we use the arctangent variant of the White generator [36, 68]. Applying (S2) to (S1) we obtain a flow equation for the Hamiltonian

$$\frac{d}{ds}H(s) = [\eta(s), H(s)]. \quad (\text{S3})$$

Integrating the differential equation (S3) yields $H(s)$.

The IMSRG transformation induces many-body interactions and operators, which must be truncated due to their computational cost. There are two approximations of the IMSRG equations used in this work, the VS-IMSRG(2) and the VS-IMSRG(3f₂) [44]. In the IMSRG(2) approximation all operators are truncated at the normal-ordered two-body level. This approximation may be systematically improved by going to the IMSRG(3) approximation, including normal-ordered three-body operators [69]. The IMSRG(3) is, however, too computationally expensive to be practical currently. As a result several approximations of the IMSRG(3) have been developed [44, 69–71], which seek to capture the leading effects of normal-ordered three-body operators in approximate ways. The IMSRG(3f₂)

does this using a modified ansatz and a factorized evaluation of the IMSRG transformation [44], allowing it to capture leading IMSRG(3) effects at the same computational cost as the IMSRG(2).

Instead of directly integrating the flow equation (S3), we solve the IMSRG equations using the Magnus expansion [72]. The unitary transformation is expressed as the exponentiation of the anti-Hermitian Magnus operator Ω

$$U(s) = e^{\Omega(s)}. \quad (\text{S4})$$

When the norm of the Magnus operator exceeds a given threshold, it is advantageous to split the transformation into two smaller unitary transformations. Consequently, Eq. (S4) becomes

$$U(s) = U(s - s_1)U(s_1) = e^{\Omega(s-s_1)}e^{\Omega(s_1)}. \quad (\text{S5})$$

Our IMSRG(2) calculations employ such a splitting approach, which can help reduce numerical errors [73], while our IMSRG(3f₂) do not [44]. The robustness of our V -factor predictions is clearly not sensitive to this choice.

Basic setup

We expand our calculations in a spherical harmonic-oscillator (HO) single-particle basis with $\hbar\omega = 16$ MeV. The basis is truncated according to $e = 2n + \ell \leq e_{\text{max}} = 12$, where n and ℓ denote the radial and orbital angular-momentum quantum numbers. Three-particle states used in the matrix elements of three-body operators are further truncated by $e_1 + e_2 + e_3 \leq E_{3\text{max}} = 18$ [74]. We employ an optimized natural orbital basis following the prescription of Ref. [75]. We solve for the natural orbital basis in the full HO single-particle basis with $e_{\text{max}} = 12$, then transform all operators to the new basis, and then truncate to a smaller model space with $e_{\text{max}}^{\text{NAT}} = 10$ before solving the IMSRG. This reduces the computational cost of the many-body calculation while delivering results that are well converged with respect to the model-space truncation.

We use the p -shell valence space for our computations of the moments of ^{10}C , $^{10}\text{B}^*$, ^{14}O , and $^{14}\text{N}^*$, and we use an sd -shell valence space for our computations of the moments of $^{26\text{m}}\text{Al}$ and ^{26}Mg . An estimate of the reference-state dependence is not included in this work. Throughout, we use the parent nucleus as the reference state.

Computation of $F_{\text{ch}}(q^2)$

We compute the translationally invariant charge form factor from the expectation value of the charge form-factor operator in Eq. (5) and by restoring translational invariance following Eq. (6). The charge form factor $F_{\text{ch}}(q^2)$ is evaluated at a set of momentum transfers q .

e_{\max}^{NAT}	$\langle r^2 \rangle$	$\langle r^4 \rangle$	$\langle r^6 \rangle$	V_{24}	V_{26}
8	8.6767(1)	111.41(3)	1863(7)	0.90666(6)	0.8397(5)
10	8.7046(1)	112.45(3)	1900(7)	0.90601(6)	0.8384(5)
12	8.7393(1)	113.86(3)	1955(8)	0.90499(6)	0.8360(6)

Table S1. The model-space size e_{\max}^{NAT} dependence of the charge-radius moments and V -factors for ^{26}Al using 1.8/2.0 (EM) with $E_{3\max} = 18$ and $\hbar\omega = 16$ MeV. The uncertainties of the moments are obtained from the GP, and the uncertainties of the V factors are estimated by propagating the moment uncertainties assuming they are independent.

For the IMSRG(2) calculations, we use values up to $q = 1040$ MeV, while for the IMSRG(3f₂) calculations we use values up to $q = 190$ MeV. Following Ref. [40], we use Gaussian-process (GP) regression to obtain a smooth representation of $F_{\text{ch}}(q^2)$ and evaluate the derivatives analytically. The lowest 25 momentum-transfer points, corresponding to approximately $q_{\max} = 0.8 \text{ fm}^{-1}$, are used as the training data for the GP.

More specifically, for the IMSRG(2) calculations, the form factor is evaluated at $q = 0, 1, 2, 3, 4, 5, 10, 15, 20, 25, 30, 35, 40, 45, 50, 60, 70, 80, 90, 100, 115, 130, 145, 160, 175, 190, 240, 290, 340, 390, 440, 490, 540, 590, 640, 690, 740, 790, 840, 890, 940, 990, 1040$ MeV. For the IMSRG(3f₂) calculations, it is evaluated at $q = 0, 1, 2, 3, 4, 5, 10, 15, 20, 25, 30, 35, 40, 45, 50, 60, 70, 80, 90, 100, 115, 130, 145, 160, 175, 190$ MeV. The interpolation uncertainty in the extracted V factors as quantified by the GP is found to be negligible. For example, for ^{26}Al with the 1.8/2.0 (EM) interaction and a model-space truncation of $e_{\max}^{\text{NAT}} = 10$, we obtain

$$V_{24} = 0.9060142 \pm 6.165 \times 10^{-5},$$

$$V_{26} = 0.8383602 \pm 5.377 \times 10^{-4}.$$

Therefore, in the final uncertainty estimation, we neglect the GP contribution to the uncertainty of the *ab initio* V factors.

To estimate the residual uncertainty associated with the basis truncation, we study the dependence on the final basis truncation e_{\max}^{NAT} . We perform the IMSRG calculations in truncated spaces with $e_{\max}^{\text{NAT}} = 8, 10$, and 12, while keeping $E_{3\max} = 18$ and $\hbar\omega = 16$ MeV fixed. The final results presented in this work are obtained with $e_{\max}^{\text{NAT}} = 10$. As shown in Table S1, increasing the model space from $e_{\max}^{\text{NAT}} = 10$ to $e_{\max}^{\text{NAT}} = 12$ changes $\langle r^2 \rangle$, $\langle r^4 \rangle$, and $\langle r^6 \rangle$ by approximately 0.40%, 1.26%, and 2.90%, respectively. The dimensionless ratios are more stable, and V_{24} and V_{26} change by only 0.11% and 0.27%, respectively, from $e_{\max}^{\text{NAT}} = 10$ to $e_{\max}^{\text{NAT}} = 12$. These results support the use of $e_{\max}^{\text{NAT}} = 10$ for the calculations reported in this work.

Details of uncertainty quantification

As stated in the main text, we adopt two different methods to assess the uncertainties in f from different sources. Details of each method are presented as follows.

Method 1

In the first method, we parameterize all charge densities using the 3pF model:

$$\rho_{\text{ch}}(r) = \frac{\rho_0(1 + wr^2/c^2)}{1 + \exp\{(r^2 - c^2)/a^2\}}, \quad (\text{S6})$$

with the parameters a , c , and w fixed to reproduce the given values of $\langle r^2 \rangle$, V_{24} and V_{26} . As we demonstrated in the main text, different choices of model only affect the central value at the 0.001% level, which is below our precision goal.

To assess the uncertainty due to the *ab initio* calculation, we fix $\langle r^2 \rangle$, Q_{EC} and compute f using the V -factors resulting from different IMSRG truncations and different Hamiltonians. Meanwhile, to assess the uncertainty due to charge radii and Q_{EC} , we compute f by varying these parameters between their central value and maximum value, one at a time, under the same *ab initio* setting [VS-IMSRG(2) with the 1.8/2.0 (EM) interaction]. The results are summarized in Table SII, SIII, SIV, from which one clearly observes that the variations of the outcome due to different *ab initio* settings are on the order of 0.001% or smaller. This is a strong demonstration of the robustness of our proposed prescription in pinning down finite size effects in f .

Method 2

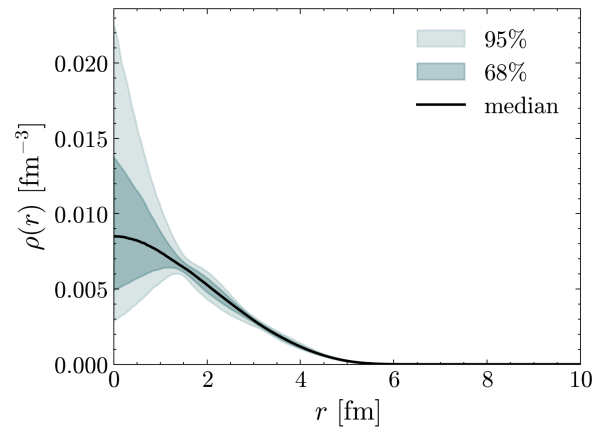


Figure S1. The combined plot of all ^{26}Al charge densities generated in Method 2.

Method	Hamiltonian	V_{24}^0	V_{26}^0	V_{24}^+	V_{26}^+	r_0 (fm)	r_+ (fm)	Q_{EC} (MeV)	f					
VS-IMSRG(2)	1.8/2.0 (EM)	0.877059	0.782291	0.890526	0.81216	2.531	2.361	1.908061	2.30231					
						2.569	2.361	1.907994	2.30154					
						2.531	2.397	1.907994	2.30165					
VS-IMSRG(2)	1.8/2.0 (EM)	0.877059	0.782291	0.890526	0.81216				2.30160					
	1.8/2.0 (EM7.5)	0.875084	0.780299	0.888204	0.809547	2.531	2.361	1.907994	2.30160					
	$\Delta\text{NNLO}_{\text{GO}}$	0.87618	0.780693	0.88906	0.807761				2.30160					
VS-IMSRG(3f ₂)	1.8/2.0 (EM)	0.883212	0.795782	0.894602	0.820906	2.531	2.361	1.907994	2.30159					
									1.8/2.0 (EM7.5)	0.876779	0.786487	0.887091	0.808138	2.30160
									$\Delta\text{NNLO}_{\text{GO}}$	0.88528	0.799844	0.894687	0.819654	2.30159

Table SII. Predicted statistical rate functions f for $^{10}\text{C} \rightarrow ^{10}\text{B}^*$. In the top three rows, we keep the *ab initio* input fixed and vary the charge radius of the $T_z = 0$ nucleus r_0 , the charge radius of the $T_z = +1$ nucleus r_+ , and the electron capture Q -value Q_{EC} between their central values and their maximum values (indicated in bold). In the middle three rows, we consider VS-IMSRG(2) predictions for the V -factors in the $T_z = 0$ nucleus, V_{24}^0 and V_{26}^0 , and the $T_z = +1$ nucleus, V_{24}^+ and V_{26}^+ , for three Hamiltonians from chiral EFT. In the bottom three rows, we consider instead VS-IMSRG(3f₂) predictions for the V -factors. Data input: $r_{\text{ch}}(^{10}\text{B}^*) = 2.531(38)$ fm, $r_{\text{ch}}(^{10}\text{Be}) = 2.361(36)$ fm, $Q_{\text{EC}} = 1.907994(67)$ MeV. Average result (only individual uncertainties larger than $5 \times 10^{-3}\%$ are displayed): $f = 2.3016(7)_{Q_{\text{EC}}(4)_{\text{scr}}}$.

Method	Hamiltonian	V_{24}^0	V_{26}^0	V_{24}^+	V_{26}^+	r_0 (fm)	r_+ (fm)	Q_{EC} (MeV)	f					
VS-IMSRG(2)	1.8/2.0 (EM)	0.891785	0.811609	0.901454	0.833964	2.623	2.508	2.831619	42.8076					
						2.632	2.508	2.831543	42.7992					
						2.623	2.517	2.831543	42.8004					
VS-IMSRG(2)	1.8/2.0 (EM)	0.891785	0.811609	0.901454	0.833964				42.7999					
	1.8/2.0 (EM7.5)	0.89479	0.817011	0.90523	0.839298	2.623	2.508	2.831543	42.7999					
	$\Delta\text{NNLO}_{\text{GO}}$	0.89178	0.810852	0.902742	0.835454				42.8000					
VS-IMSRG(3f ₂)	1.8/2.0 (EM)	0.892212	0.812461	0.901403	0.833825	2.623	2.508	2.831543	42.7998					
									1.8/2.0 (EM7.5)	0.894959	0.817085	0.907859	0.844733	42.8002
									$\Delta\text{NNLO}_{\text{GO}}$	0.892575	0.813121	0.904046	0.837868	42.8001

Table SIII. Same as Table SII but for $^{14}\text{O} \rightarrow ^{14}\text{N}^*$. Data input: $r_{\text{ch}}(^{14}\text{N}^*) = 2.623(9)$ fm, $r_{\text{ch}}(^{14}\text{C}) = 2.508(9)$ fm, $Q_{\text{EC}} = 2.831543(76)$ MeV. Average result: $f = 42.800(8)_{Q_{\text{EC}}(6)_{\text{scr}}}$.

Method	Hamiltonian	V_{24}^0	V_{26}^0	V_{24}^+	V_{26}^+	r_0 (fm)	r_+ (fm)	Q_{EC} (MeV)	f					
VS-IMSRG(2)	1.8/2.0 (EM)	0.90602	0.838353	0.907052	0.839918	3.132	3.030	4.23287	478.128					
						3.140	3.030	4.23272	478.002					
						3.030	3.033	4.23272	478.034					
VS-IMSRG(2)	1.8/2.0 (EM)	0.90602	0.838353	0.907052	0.839918				478.027					
	1.8/2.0 (EM7.5)	0.910733	0.846652	0.910906	0.846836	3.132	3.030	4.23272	478.016					
	$\Delta\text{NNLO}_{\text{GO}}$	0.908996	0.8426	0.909454	0.843408				478.019					
VS-IMSRG(3f ₂)	1.8/2.0 (EM)	0.905932	0.839231	0.906857	0.840003	3.132	3.030	4.23272	478.029					
									1.8/2.0 (EM7.5)	0.912871	0.851619	0.913008	0.851465	478.015
									$\Delta\text{NNLO}_{\text{GO}}$	0.909909	0.845447	0.910135	0.845083	478.019

Table SIV. Same as Table SII but for $^{26}\text{Al} \rightarrow ^{26}\text{Mg}$. Data input: $r_{\text{ch}}(^{26}\text{Al}) = 3.132(8)$ fm, $r_{\text{ch}}(^{26}\text{Mg}) = 3.030(3)$ fm, $Q_{\text{EC}} = 4.23272(15)$ MeV. Average result: $f = 478.02(10)_{Q_{\text{EC}}(8)_{\text{scr}}(3)_{r_{\text{Al}}}}$.

Transition	Mean f	Std. dev.	95% interval
$^{26}\text{mAl} \rightarrow ^{26}\text{Mg}$	478.029	0.040	[477.954, 478.107]
$^{10}\text{C} \rightarrow ^{10}\text{B}^*$	2.30150	0.00006	[2.30137, 2.30162]
$^{14}\text{O} \rightarrow ^{14}\text{N}^*$	42.8010	0.0008	[42.7994, 42.8025]

Table S V. Summary of sampled statistical rate functions. Intervals are empirical central probability intervals over the density ensemble.

In the second method, we start with the IMSRG form factor results for the different interactions and obtain the V -factors using a Gaussian process. Then, we create a family of functions by exponentiating a set of radial Gaussians

$$g(r) = \sum_a c_a \exp(-(r - R_a)^2/s_a^2), \quad (\text{S7})$$

whose coefficients c_a are drawn randomly from a normal distribution. The widths are constant $s_a = 1$ fm and the centers R_a are evenly spaced between the origin and 12 fm. We exponentiate these function to obtain positive definite base densities

$$\rho_{\text{base}}(r) = N_{\text{base}} \exp(g(r))R(r), \quad (\text{S8})$$

where N_{base} is a normalization factor ensuring that ρ_{base} is normalized to one, and $R(r)$ is a regulator function that smoothly cuts off the density at a large distance.

We then use an exponential factor with Lagrange multipliers λ_2, λ_4 and λ_6 to create from this family of base densities ρ_{base} new densities that return the correct charge radius and moment ratios. Specifically,

$$\rho_\lambda(r) = N_\lambda \rho_{\text{base}} \exp(\lambda_2 r^2 + \lambda_4 r^4 + \lambda_6), \quad (\text{S9})$$

where N_λ is again a normalization factor. The λ s are obtained through a nonlinear least squares fit.

Figure S1 provides an illustration of the family of charge densities generated with the method above. We compute values of f by sampling the densities that were generated this way. This leads to the histogram in Fig. 3. The final numerical result is given in Table S V, where the standard deviation represents collectively the uncertainty from the charge radii, V -factors and the density models. We find excellent agreement between the two methods, in both the central values and uncertainties.